Chemical Science

ROYAL SOCIETY OF CHEMISTRY

EDGE ARTICLE

View Article Online
View Journal | View Issue

Cite this: *Chem. Sci.*, 2022, **13**, 257

All publication charges for this article have been paid for by the Royal Society of Chemistry

Unexpected role of electronic coupling between host redox centers in transport kinetics of lithium ions in olivine phosphate materials

Yu Gao,[ac] Jun Huang,†*[b] Yuwen Liu[a] and Shengli Chen *[a]

Received 30th September 2021
Accepted 1st December 2021

DOI: 10.1039/d1sc05402c

rsc.li/chemical-science

The discrepancy between the trend in the diffusion coefficient of a lithium ion (D_{Li^+}) and that in the activation energy of ion hopping signals hidden factors determining ion transport kinetics in layered olivine phosphate materials ($LiMPO_4$). Combining density functional theory (DFT) calculations and the Landau–Zener electron transfer theory, we unravel this hidden factor to be the electronic coupling between redox centers of the host materials. The ion transport process in $LiMPO_4$ is newly described as an ion-coupled electron transfer (ET) reaction, where the electronic coupling effect on D_{Li^+} is considered by incorporating the electronic transmission coefficient into the rate constant of the transfer reaction. The new model and DFT calculation results rationalize experimental values of D_{Li^+} for various $LiMPO_4$ (M = Fe, Mn, Co, Ni) materials, which cannot be understood solely by the calculated activation barrier of ion hopping. Interestingly, the electronic coupling between host redox centers is found to play an essential role. Particularly, the sluggish ion mobility in $LiFePO_4$ is due to a very weak electronic coupling. The obtained insights imply that one can improve the rate performance of intercalation materials for metal-ion batteries through modifying the electronic coupling between redox centers of host materials.

1. Introduction

Ion transport in intercalation compounds is an elementary process underpinning rechargeable metal-ion batteries that drive the paradigm shift of storing sustainable and clean energy. $LiFePO_4$, a layered olivine phosphate material composed of earth-abundant and non-toxic elements, exhibits numerous merits such as low cost, high structural stability, and competitive electrochemical performance, and therefore constituting one of the mainstream cathode materials in rechargeable lithium-ion batteries.[1–4] Key challenges faced by $LiFePO_4$ include low electronic conductivity (10^{-10}–10^{-15} S cm^{-1}) and ionic mobility, hindering the realization of high-power devices.[5–8] A practical consequence of this is that the charging time of electrical vehicles powered by Li_xMPO_4 is much longer compared to the fuel filling time of conventional fossil-fuelled cars.[9–12]

Therefore, the mechanism and kinetics of ion transport in $LiFePO_4$ has attracted research interest for decades from both computational and experimental sides in the past few years. In experimental studies, the diffusion coefficient of lithium ions, D_{Li^+}, in pure $LiFePO_4$ is found to vary between 10^{-13} and 10^{-15} cm^2 s^{-1},[13–17] while theoretical calculations have arrived at numbers that are several orders of magnitude higher.[18–25] Such discrepancy is rooted in the belief that the lithium ion transport through diffusion in the lattice frame of intercalation solids has led to the use of the activation barrier of ion hopping (E_a) to estimate D_{Li^+} according to the following Arrhenius type of kinetic equation:[18]

$$D_{Li^+} = D_0 \exp\left(-\frac{E_a}{k_B T}\right) \quad (1)$$

where the pre-exponential factor D_0 represents the activationless (free) diffusion coefficient. First-principles-based computations mostly have given relatively small numbers for E_a. The unreasonably high D_{Li^+} values estimated by E_a thus suggest that the Li^+ transport in $LiFePO_4$ is far more complicated than the simple particle diffusion process described by eqn (1).

Indeed, there are evidences showing that transport of electrons and Li^+ ions is closely coupled in $LiFePO_4$. The electron-coupled Li^+ transport[26,27] (or equivalently, Li^+-coupled electron transfer) mechanism explains why the carbon coating technique,[28–30] aimed initially at improving the electronic conductivity, fortuitously increases the ionic diffusivity in $LiFePO_4$. The first experimental clue of the electron-coupled Li^+ transport mechanism was reported by Ellis *et al.*[27] They found in Mossbauer measurements that the isomer shift corresponding to the

[a]Hubei Key Laboratory of Electrochemical Power Sources, College of Chemistry and Molecular Science, Wuhan University, Wuhan 430072, China. E-mail: slchen@whu.edu.cn

[b]College of Chemistry and Chemical Engineering, Central South University, Changsha 410083, China. E-mail: jhuangelectrochm@qq.com

[c]School of Chemistry and Materials Engineering, Fuyang Normal University, Fuyang, Anhui 236041, China

† Present address: Institute of Theoretical Chemistry, Ulm University, 89069 Ulm, Germany.

average Fe^{2+}/Fe^{3+} environment is closely correlated with the Li^+ disorder in the lattice, and that Li^+ transport is correlated with the vibrational modes of the phosphate lattice. First-principles calculations by Maxisch *et al.* revealed that the activation energy of Li^+-coupled ET is much lower than that of the decoupled transfer process.[31] In addition, nonadiabatic molecular dynamics simulations by Tao *et al.* have also revealed that the Li^+ diffusion can be significantly enhanced upon the formation of a small polaron.[26]

Although widespread experimental and computational efforts underscore the ion-coupled ET nature of Li^+ diffusion in $LiFePO_4$, there lacks a quantitative description of Li^+ transport kinetics in this coupled charge transfer mechanism. Herein, we propose a kinetic model for ion transport in intercalation solids by describing it as an ion-coupled ET reaction. The electronic effect is incorporated into the model formula by using the Landau–Zener ET theory, which allows the ion transport kinetics to be directly correlated with the electronic coupling between the host redox centers. In the meantime, first-principles calculations based on the density functional theory (DFT) are performed to determine the key parameters in the model formula. The comparison between the model results and experimental data clearly demonstrates the determining role of electronic coupling in the ion dynamics of $LiMPO_4$, and thus providing guidance for rational design of ion-intercalation electrode materials.

2. Results and discussion

2.1 Microkinetic model

$LiMPO_4$ has an olivine structure with O forming a distorted hexagonal close-packed (hcp) framework which accommodates Li and M at the octahedral interstices and P at the tetrahedral interstices respectively (Fig. 1 for $LiFePO_4$). During charging (discharging) processes, Li ions are removed (added) topotactically, maintaining the topology of the MPO_4 framework. There are three possible hopping paths for Li ions, corresponding to the motion along the *b* direction in the hexagonal *a*–*b* planes of the oxygen hcp host, that between the *b* channels in the neighboring hexagonal planes along the *c* axis, and that between the neighboring *b* channels in the *a*–*b* plane.[18] DFT-based nudged elastic band calculations have shown that Li hopping along the *b* direction has the lowest energetic barrier,[18] which was later confirmed in experiments.[32]

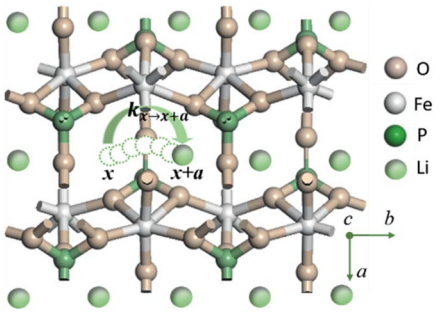

Fig. 1 Illustration of Li^+ transport *via* a curved trajectory between adjacent sites along the *b* direction of $LiMPO_4$.

Considering that lithium ion transport in $LiMPO_4$ is mainly along the *b*-direction,[3–8,18] we can model it as a one-dimensional (1-D) ion hopping process. We adopt the recent idea that the ion hopping in concentrated media corresponds to an ion-vacancy coupled transfer reaction, that is, $I_x - V_x \leftrightarrow I_{x\pm a} - V_{x\pm a}$.[33,34] This underlying idea is that the appearance of an ion at position *x* is accompanied by the loss of a vacancy there. The rate of this ion-vacancy coupled transfer reaction can be formulated according to the law of mass action, that is[33,34]

$$\frac{\partial c_x}{\partial t} = k_{x+a\to x}c_{x+a}(1-vc_x) + k_{x-a\to x}c_{x-a}(1-vc_x) - k_{x\to x-a}c_x(1-vc_{x-a}) - k_{x\to x-a}c_x(1-vc_{x-a}) \quad (2)$$

where c_x refers to the number density of ions at position *x*, $k_{x\to y}$ represents the rate constant of ion transfer from position *x* to *y* ($y = x + a$, or $x - a$), *a* is the average distance of ion hopping, and *v* is the average volume excluded by an ion ($v = a$ in a 1-D system). The product vc_x thus represents the volume fraction occupied by ions at position *x*, and the term $(1 - vc_x)$ is that of vacancies accordingly.

In the spirit of transition state theory and the Brønsted–Evans–Polanyi (BEP) relationship, the rate constants $k_{x\to y}$ can be expressed as,

$$k_{x\to y} = k^0 \exp\left(-\frac{\beta\left(\mu_y^0 - \mu_x^0\right)}{k_B T}\right) \quad (3)$$

where μ_x^0 refers to the standard chemical potential of ions at position *x*, β (≈ 0.5) is the BEP coefficient (also called the symmetric factor), and the pre-factor k^0, the so-called standard rate constant, refers to the equal rate constants of the forward and backward hopping processes under thermodynamic neutral conditions, *i.e.*, $\mu_y^0 = \mu_x^0$. When the standard chemical potential varies very mildly so that $\mu_y^0 - \mu_x^0 \ll k_B T$, taking the first two items of the Taylor expansion of $k_{x\to y}$ into eqn (2), we have the following near-equilibrium thermodynamic equation for ion transport,[33,34]

$$\frac{\partial c_x}{\partial t} = \nabla\left(\frac{D}{k_B T}c_x(1-vc_x)\nabla\mu_x\right) \quad (4)$$

where $D = a^2k^0$ is the diffusion coefficient. Thus, the ion diffusion coefficient is linked to the standard rate constant of an ion hopping reaction. According to the transition state theory, k^0 can be related to the activation energy of ion hopping (E_a) as $k^0 = 1/2\tau_0 \exp(-E_a/k_B T)$,[32] where τ_0 refers to the average time interval of the ion hopping events. The factor 2 in the denominator of the right-hand side is the consequence of activation entropy when considering that the transition state occupies two vacancies.[33,34] It can also be understood that a transition state has the equal probability of 1/2 to go forward and backward. Thus, *D* can be formulated as,

$$D = \frac{a^2}{2\tau_0}\exp\left(-\frac{E_a}{k_B T}\right) \quad (5)$$

In the case when the activation barrier is negligibly small, *e.g.*, the free diffusion, one has $D = a^2/2\tau_0$, which is exactly the result of Einstein's diffusion theory for Brownian motion.

For the electron-coupled ion hopping process, the value of τ_0 should be co-determined by electronic and nuclear factors. As a first approximation, we use $\tau_0 = (\nu_n\kappa_{el})^{-1}$, where ν_n is the effective frequency of nuclear motion and κ_{el} the electronic transmission coefficient. Considering that the ion hopping event is mainly a result of the vibration of the M–O bond, we assign the typical frequency (10^{13} s^{-1}) of the normal vibration of the M–O bond to ν_n.[35] To estimate κ_{el}, we use the Landau–Zener formula,[36–38] that is, $\kappa_{el} = \frac{2(1-\exp(-\nu_{el}/2\nu_n))}{2-\exp(-\nu_{el}/2\nu_n)}$, where $\nu_{el} = \frac{2H_{AB}{}^2}{h}\left(\frac{\pi^3}{\lambda k_B T}\right)^{1/2}$ is the electron hopping frequency at the transition state, λ is the configurational reorganization energy of electron transfer (Fig. 2), and H_{AB} is the electronic coupling matrix element which represents the electronic coupling strength between the redox centers,[39] which are the neighboring transition metal centers in $LiMPO_4$ (Fig. 2). Thus, we have the following formula for the ion diffusion coefficient:

$$D = a^2\nu_n \exp\left(-\frac{E_a}{k_B T}\right) \frac{1-\exp\left(-\frac{2H_{AB}{}^2}{h}\left(\frac{\pi^3}{\lambda k_B T}\right)^{1/2}\Big/ 2\nu_n\right)}{2-\exp\left(-\frac{2H_{AB}{}^2}{h}\left(\frac{\pi^3}{\lambda k_B T}\right)^{1/2}\Big/ 2\nu_n\right)} \quad (6)$$

Depending on the magnitude of H_{AB}, an ET process can be adiabatic or nonadiabatic. The adiabatic ET system has a large H_{AB}, which means $\nu_{el} \gg \nu_n$, and therefore $\kappa_{el} \approx 1$. In this case, τ_0 is mainly determined by the nuclei factor and the ion diffusion coefficient reads $D = (1/2)a^2\nu_n \exp(-E_a/k_BT)$, which corresponds to a thermally activated diffusion process with an Arrhenius type of kinetics as described in eqn (1) and is negligibly effected by the electronic effect. For a nonadiabatic ET with small H_{AB}^2 and κ_{el}, the ion diffusion coefficient reads $D = (1/2)a^2\nu_{el} \exp(-E_a/k_BT)$, and can be reformulated as,

$$D = \frac{1}{2}a^2 \exp\left(-\frac{E_a}{k_B T}\right) \frac{2H_{AB}{}^2}{h}\left(\frac{\pi^3}{\lambda k_B T}\right)^{1/2} \quad (7)$$

where a proportional relationship is found between D and H_{AB}^2. In other words, E_a and H_{AB} should be used together to describe the ion transport properties in $LiMPO_4$.

Due to the fact that the adjacent redox centers in $LiMPO_4$ are separated by relatively large distance, the electronic interactions should be weak, making the ET process mostly nonadiabatic. Therefore, the key parameters determining the Li^+ diffusion coefficient include H_{AB}, λ, and E_a.

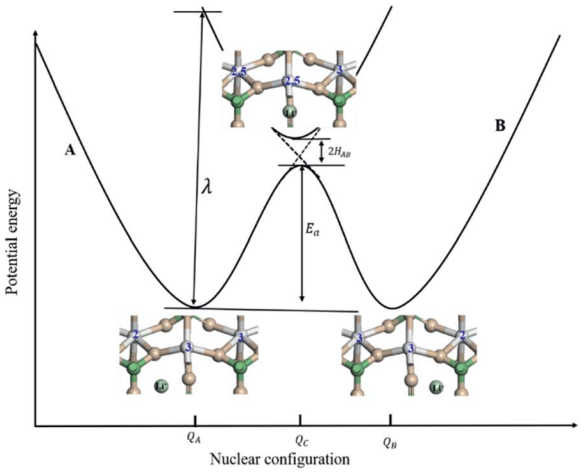

Fig. 2 Schematic illustration of the potential energy surface for Li^+-coupled electron transfer (ET) reaction in $LiMPO_4$ as a function of the nuclear configuration. The solid and dashed curves represent the adiabatic and nonadiabatic cases. Q_A and Q_B are the equilibrium nuclear coordinates of the states A and B, respectively, and Q_C is the nuclear coordinate corresponding to the lowest energy on the crossing seam surface. λ is the intramolecular reorganization energy, E_a is the activation energy for the adiabatic ET, and H_{AB} represents the strength of electronic coupling between neighboring transition metal centers at the transition state.

2.2 DFT-based parameterization

We employed the DFT calculations to determine these model parameters for Li^+ transport in $LiMPO_4$ (M = Fe, Mn, Co, Ni). Specifically, minimum energy pathways (MEPs) and saddle points of Li^+ hopping were obtained with the climbing-image nudged elastic band (CINEB) method[40] in the PWscf (Plane-Wave Self-Consistent Field) module in Quantum ESPRESSO with the ultrasoft pseudopotentials for nuclei and core electrons (see details in the Methods section).[41] Usually, 5–7 images are interpolated in CINEB computations to determine the transition states and activation barriers of ion migration in solid crystals. Considering the relatively simple 1-D hopping of Li ions and small change of the solid structure in the hopping process of Li ions in $LiMPO_4$, five images are adequate to identify the transition states.[18,20] Therefore, we interpolated five images between the starting and end points in the ion transport process to simulate the intermediate states, with the positions of the starting point and the end point fixed. This can significantly reduce the computation cost without losing the accuracy. The transition states obtained agree with those reported in the literature.[18,20]

The values of H_{AB} were determined by using a large-scale parallel multiconfigurational self-consistent field (MCSCF) implemented in the NWChem computational chemistry code,[42] and the bases are set as 6-31g** for P, O and Li, and LANL2DZ ECP for Fe, respectively. In H_{AB} calculations, the reactant and the product had the same configurations as those of the transition state obtained in the CINEB method, but the charges were assigned differently to distinguish the reactant, transition state and product of an ET process (Fig. 2).

A 1a × 2b × 1c (S.G. *Pnma*) supercell was used in all calculations. The cell contains 8 Li^+ sites in total, with 7 sites filled with Li^+, thus having a composition of $Li_{0.875}MPO_4$, which is in consistence with the model in previous studies so that the calculated activation barriers are comparable with the reported values.

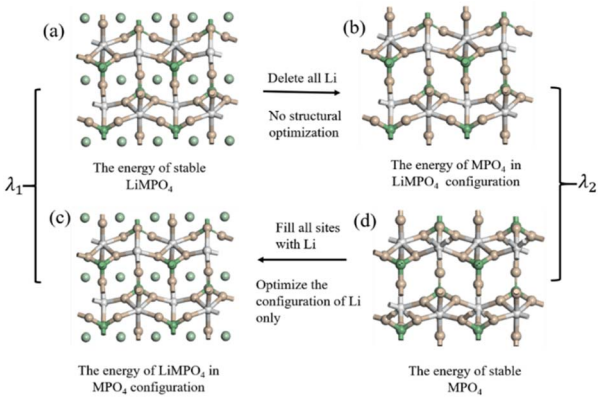

Fig. 3 Schematic diagram for computation of the configuration reorganization energies of the reaction in $LiMPO_4$.

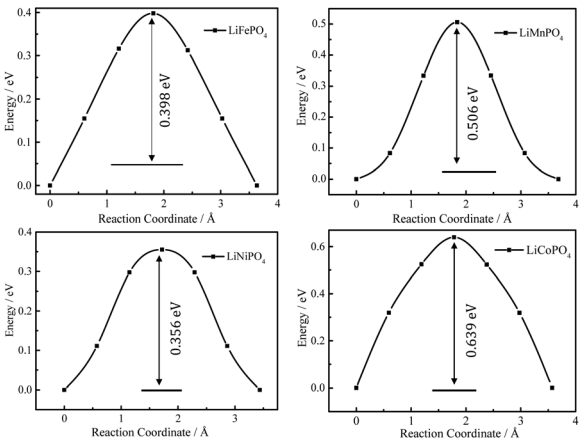

Fig. 4 DFT-calculated energy profiles of Li^+ hopping along the MEP between adjacent Li sites in $Li_{0.875}MPO_4$.

The configuration reorganization energies (λ) were calculated using the procedure shown in Fig. 3. First, structural optimization was performed to obtain the stable configurations of $LiMPO_4$ (Fig. 3(a)) and MPO_4 (Fig. 3(d)), which have energies of E_1 and E_2 respectively. Then, the $LiMPO_4$ structure was obtained by filling Li atoms in the stable configuration of MPO_4 without altering the host structure (Fig. 3(c)), giving a total energy of E_3; and the structure of MPO_4 was obtained by simply removing all Li atoms from the stable configuration of MPO_4 while leaving other constituents unaltered (Fig. 3(b)), which gives an energy of E_4. Thus, $\lambda_1 = (E_3 - E_1)$ is assigned to the reorganization energy of a $LiMPO_4$ site in an ET process, and $\lambda_2 = (E_4 - E_2)$ to that of a MPO_4 site. The total configuration reorganization energy for the ET process between a pair of $LiMPO_4$ and MPO_4 sites is the sum of λ_1 and λ_2, namely, $\lambda = \lambda_1 + \lambda_2$.

Fig. 4 shows the energy profiles of MEPs of Li^+ hopping between two adjacent sites along the b axis in $Li_{0.875}MPO_4$ (M = Fe, Mn, Ni, and Co) calculated using the CINEB method, with the inset numbers indicating the corresponding E_a values. These values (0.40 eV for $LiFePO_4$, 0.51 eV for $LiMnPO_4$, 0.64 eV for $LiCoPO_4$, and 0.36 eV for $LiNiPO_4$) are close to that obtained from the DFT+U calculations by Dathar *et al.* (0.47 eV for $LiFePO_4$),[20] but differ from those obtained from the Born model of solids (0.55 eV for $LiFePO_4$, 0.62 eV for $LiMnPO_4$, 0.49 eV for $LiCoPO_4$, and 0.44 eV for $LiNiPO_4$)[23] and those obtained from the DFT calculations without Hubbard correction for strongly correlated d electrons (0.27 eV for $LiFePO_4$, 0.25 eV for $LiMnPO_4$, 0.36 eV for $LiCoPO_4$, and 0.13 eV for $LiNiPO_4$).[18]

2.3 Electronic coupling

Given the DFT-calculated parameters of a^2, H_{AB}, λ, and E_a, we estimated the diffusion coefficients of Li^+ using eqn (6). The DFT-calculated parameters and the corresponding theoretical diffusion coefficients ($D_{Li^+}^{cal}$) are listed in Table 1, where the experimental diffusion coefficients $D_{Li^+}^{exp}$ taken from the literature are also given for comparison. It is revealing to note that $LiFePO_4$ and $LiNiPO_4$ show a difference of three orders in experimentally-measured diffusion coefficients, although they have very close E_a values. Besides, compared with $LiMnPO_4$, $LiCoPO_4$ has a higher experimental diffusion coefficient in spite of a larger E_a. Such anomalies indicate that the activation energy inadequately predicts the ion transport kinetics in olivine phosphate materials as described in eqn (1).

The inconsistency between diffusion coefficients and hopping activation barriers can be understood when the electronic coupling factors are considered. One can see that the H_{AB} is much higher for $LiNiPO_4$ compared with $LiFePO_4$, and higher for $LiCoPO_4$ compared with $LiMnPO_4$. The ($D_{Li^+}^{cal}$) values estimated by considering the electronic factor through the Landau–Zener ET theory reasonably agree with the experimental data. This further confirms the electron-coupled ion transfer mechanism of Li^+ transport in these materials and the essential role of the electronic coupling between transition metal centers.

It is also worthwhile mentioning that the potential energy profiles shown in Fig. 4 are in general not parabolic, as assumed in the standard ET theory by Marcus.[50] We note that the parabolic potential energy curves are expected only for outer-sphere

Table 1 Calculated values of the activation barriers, the strength of electronic coupling matrix elements, the configuration reorganization energies, and the diffusion coefficients for Li^+ transport in $Li_{0.875}MPO_4$

M	a (Å)	E_a (eV)	$\lambda/4$ (eV)	H_{AB} (eV)	ν_{el} (s^{-1})	$D_{Li^+}^{cal}$ ($cm^2\ s^{-1}$)	$D_{Li^+}^{exp}$ ($cm^2\ s^{-1}$)
Fe	3.634	0.398	0.390	1.39×10^{-3}	2.59×10^{10}	4.43×10^{-13}	10^{-15}–10^{-13} (ref. 21–25)
Mn	3.684	0.506	0.815	0.24×10^{-3}	5.35×10^{8}	2.08×10^{-15}	10^{-15}–10^{-14} (ref. 8 and 43–45)
Co	3.572	0.639	0.179	4.91×10^{-3}	4.78×10^{11}	6.06×10^{-15}	10^{-15}–10^{-12} (ref. 46 and 47)
Ni	3.439	0.356	0.197	3.25×10^{-2}	1.99×10^{13}	1.24×10^{-9}	10^{-11}–10^{-9} (ref. 48 and 49)

ET processes involving no molecular structural change other than harmonic relaxation. Nevertheless, the ET process here is accompanied by the nuclear motion of Li atoms, which changes the electronic environment during the course as well. Consequently, the deviation of the real energy profiles from the parabolic curves is unsurprising. As a direct consequence, E_a and λ does not satisfy the relationship of $E_a = \lambda/4$ as predicted by the classical Marcus theory (Table 1). More specifically, the deviation is much more pronounced for $LiNiPO_4$ and $LiCoPO_4$ than that for other compounds considered here, suggesting a unusual charge transfer behavior for $LiNiPO_4$ and $LiCoPO_4$.

It is now clear that, owing to the ion-coupled ET nature, neither the thermal diffusion nor the classical ET theory is insufficient for a quantitative description of ion transport kinetics in olivine phosphate materials of $LiMPO_4$. A comprehensive model for the ion-coupled ET process in condensed matters should include the detailed electronic ion–host interactions and their effects on the structural relaxation of the host metal–ligand systems, which are beyond the scope of this work. What we show here is that modelling the ion transport in terms of the hoping reaction kinetics provides a route to access this coupled transfer mechanism. Despite the great approximation, the electron coupling effect can be included in the ion transport kinetics by simply incorporating the electronic transmission coefficient given by Landau–Zener theory into the pre-exponential frequency factor of the rate constant of the hopping reaction. This allows the apparent diffusion coefficient of Li^+ in $LiMPO_4$ to be reasonably estimated using the parameters obtained from first-principles computations.

3. Conclusions

We have developed a new theoretical model for Li^+ transport in olivine phosphate materials of $LiMPO_4$, which is described as an ion-coupled electron transfer process. In particular, the effect of electronic coupling between host redox centers on the ion transport kinetics is emphasized and can be described using the Landau–Zener theory. In this model, the diffusion coefficient is co-determined by the electronic coupling matrix element between the neighboring transition metal centers, the configuration reorganization energy of electron transfer, and the activation energy of ion hopping. The values of these parameters can be obtained from DFT calculations. The model can rationalize the anomalous trend of diffusion coefficients of Li^+ in $LiMPO_4$ (M = Fe, Mn, Co, Ni), which cannot be understood solely by the activation barrier of ion hopping. It is revealed that the electron coupling plays a vital role. The electron-transfer perspective of ion transport in $LiMPO_4$ opens new pathways to design high-performance ion intercalation materials for metal-ion batteries.

4. Computations details

Spin-polarized DFT calculations were performed using Quantum Espresso with the ultrasoft pseudopotentials for nuclei and core electrons.[41] Generalized gradient approximation (GGA) in the parameterization of the Perdew–Burke–Ernzerhof (PBE) functional was used to describe the exchange–correlation and Hubbard-type correction U was taken into account due to the strongly correlated nature of the Fe 3d electrons.[51] As recommended in a previous study, the effective U values for LiMPO4 are set to 4.3 eV, 4.5 eV, 5.7 eV, and 5.1 eV for M = Fe, Mn, Co, and Ni, respectively.[52] A kinetic energy cutoff of 30 Ry and a charge-density cutoff of 300 Ry were used in all calculations. Geometry optimization was performed by using BFGS minimization until all the forces acting on each atom were below 10^{-3} Ry per Bohr and the total energy was converged to within 10^{-6} Ry. The Brillouin-zones were sampled with a 12 × 5 × 6 *k*-point mesh for a 1a × 2b × 1c (S.G. *Pnma*) supercell containing 8 Li sites.

Data availability

The data that support the findings of this study are available on request from the corresponding author.

Author contributions

SC conceived the project. YG, JH and SC derived the model equations. YG performed the DFT calculations. YL discussed the derivation and results. YG, JH, and SC wrote the paper. All authors have given approval to the final version of the manuscript.

Conflicts of interest

There are no conflicts to declare.

Acknowledgements

This work was supported by the National Natural Science Foundation of China (21673163, 21802170).

Notes and references

1 M. S. Whittingham, *Chem. Rev.*, 2004, **104**, 4271–4301.
2 J. B. Goodenough and Y. Kim, *Chem. Mater.*, 2010, **22**, 587–603.
3 J. B. Goodenough, *Acc. Chem. Res.*, 2013, **46**, 1053–1061.
4 B. C. Melot and J.-M. Tarascon, *Acc. Chem. Res.*, 2013, **46**, 1226–1238.
5 A. Padhi, K. S. Nanjundaswamy and J. B. Goodenough, *J. Electrochem. Soc.*, 1997, **144**, 1188–1194.
6 A. Yamada, S. C. Chung and K. Hinokuma, *J. Electrochem. Soc.*, 2001, **148**, A224–A229.
7 S. Y. Chung, J. T. Blocking and Y. M. Chiang, *Nat. Mater.*, 2002, **1**, 123–128.
8 C. Delacourt, L. Laffont, R. Bouchet, C. Wurm, J. B. Leriche, J. M. Morcrette and C. Masquelier, *J. Electrochem. Soc.*, 2005, **152**, A913–A921.
9 R. Chandrasekaran, *J. Power Sources*, 2014, **271**, 622–632.
10 B. Kang and G. Ceder, *Nature*, 2009, **458**, 190–193.
11 H. B. Shu, M. F. Chen and F. e. a. Wen, *Electrochim. Acta*, 2015, **152**, 368–377.

12 K. Kirshenbaum, D. C. Bock and C. e. a. Lee, *Science*, 2015, **347**, 149–154.
13 S. Franger, F. Le Cras, C. Bourbon and H. Rouault, *Electrochem. Solid-State Lett.*, 2002, **5**, A231–A233.
14 P. P. Prosini, M. Lisi, D. Zane and M. Pasquali, *Solid State Ionics*, 2002, **148**, 45–51.
15 R. Amin, P. Balaya and J. Maier, *Electrochem. Solid-State Lett.*, 2007, **10**, A13–A16.
16 R. Amin, J. Maier, P. Balaya, D. P. Chen and C. T. Lin, *Solid State Ionics*, 2008, **179**, 1683–1687.
17 H. Liu, C. Li, H. P. Zhang, L. J. Fu, Y. P. Wu and H. Q. Wu, *J. Power Sources*, 2006, **159**, 717–720.
18 D. Morgan, A. Van der Ven and G. Ceder, *Electrochem. Solid-State Lett.*, 2004, **7**, A30–A32.
19 C. Kuss, G. Liang and S. B. Schougaard, *J. Mater. Chem.*, 2012, **22**, 24889–24893.
20 G. K. P. Dathar, D. Sheppard, K. J. Stevenson and G. Henkelman, *Chem. Mater.*, 2011, **23**, 4032–4037.
21 R. Kutteh and M. Avdeev, *J. Phys. Chem. C*, 2014, **118**, 11203–11214.
22 M. S. Islam, D. J. Driscoll, C. A. J. Fisher and P. R. Slater, *Chem. Mater.*, 2005, **17**, 5085–5092.
23 C. A. J. Fisher, V. M. H. Prieto and M. S. Islam, *Chem. Mater.*, 2008, **20**, 5907–5915.
24 K. Hoang and M. Johannes, *Chem. Mater.*, 2011, **23**, 3003–3013.
25 S. E. Boulfelfel, G. Seifert and S. Leoni, *J. Mater. Chem.*, 2011, **21**, 16365–16372.
26 G. H. Tao, *J. Phys. Chem. C*, 2016, **120**, 6938–6952.
27 B. Ellis, L. K. Perry and D. H. e. a. Ryan, *J. Am. Chem. Soc.*, 2006, **128**, 11416–11422.
28 H. Huang, S. C. Yin and L. F. Nazar, *Electrochem. Solid-State Lett.*, 2001, **10**, A170–A172.
29 P. S. Herle, B. Ellis, N. Coombs and L. F. Nazar, *Nat. Mater.*, 2004, **3**, 147–152.
30 N. D. Trinh, G. Liang and M. e. a. Gauthier, *J. Power Sources*, 2012, **200**, 92–97.
31 T. Maxisch, F. Zhou and G. Ceder, *Phys. Rev. B: Condens. Matter Mater. Phys.*, 2006, **73**, 104301.
32 S. Nishimura, G. Kobayashi, K. Ohoyama, R. Kanno, M. Yashima and A. Yamada, *Nat. Mater.*, 2008, **7**, 707–711.
33 Y. Gao, J. Huang, Y. W. Liu, J. W. Yan, B. W. Mao and S. L. Chen, *Sci. China: Chem.*, 2019, **62**, 515–520.
34 Z. Zhang, Y. Gao, S. Chen and J. Huang, *J. Electrochem. Soc.*, 2019, **167**, 013519.
35 N. Sutin, *Acc. Chem. Res.*, 1982, **15**, 275–282.
36 B. S. Brunschwig, J. Logan, M. D. Newton and N. Sutin, *J. Am. Chem. Soc.*, 1980, **102**, 5798–5809.
37 M. D. Newton and N. Sutin, *Annu. Rev. Phys. Chem.*, 1984, **35**, 437–480.
38 J. Frank and E. G. Dymond, *Trans. Faraday Soc.*, 1926, **21**, 536.
39 E. U. Condon, *Phys. Rev.*, 1928, **32**, 858.
40 G. Henkelman, B. P. Uberuaga and H. Jónsson, *J. Chem. Phys.*, 2000, **113**, 9901–9904.
41 G. Mills and H. Jónsson, *Phys. Rev. Lett.*, 1994, **72**, 1124.
42 A. Farazdel, M. Dupuis, E. Clementi and A. Aviram, *J. Am. Chem. Soc.*, 1990, **112**, 4206–4214.
43 F. Wen, H. L. Shu and Y. Y. Zhang, *Electrochim. Acta*, 2016, **214**, 85–93.
44 L. F. Zhang, Q. Qu, L. Zhang and H. H. Zheng, *J. Mater. Chem. A*, 2014, **2**, 711–719.
45 N. H. Kwon, T. Drezen, I. Exnar, I. Teerlinck, M. Isono and M. Graetzel, *Electrochem. Solid-State Lett.*, 2006, **9**, A277–A280.
46 J. Xie, N. Imanishi, T. Zhang, A. Hirano, Y. Takeda and O. Yamamoto, *J. Power Sources*, 2009, **192**, 689–692.
47 S. Brutti, J. Manzi, D. Meggiolaro, F. M. Vitucci, A. Paolone and O. Palumbo, *J. Mater. Chem. A*, 2017, **5**, 14020–14030.
48 S. Jun, N. Hiroshi and H. Masashi, *Phys. Rev. B: Condens. Matter Mater. Phys.*, 2012, **85**, 054111.
49 Y. Zhang, Y. Pan, J. Liu, G. Wang and D. X. Cao, *Chem. Res. Chin. Univ.*, 2015, **31**, 117–122.
50 R. A. Marcus and N. Sutin, *Biochim. Biophys. Acta*, 1985, 265–322.
51 J. P. Perdew, K. Burke and M. Ernzerhof, *Phys. Rev. Lett.*, 1996, **77**, 3865–3868.
52 S. L Shang, Y. Wang, X. D. Mei and Z. K. Liu, *J. Mater. Chem.*, 2012, **22**, 1142–1149.